PHYSICAL REVIEW B VOLUME 38, NUMBER 3 15 JULY 1988-II

Strained Si/Ge superlattices: Structural stability, growth, and electronic properties

S. Ciraci* and Inder P. Batra
IBM Research Division, Almaden Research Center, Mail Stop K33/801, 650 Harry Road, San Jose, California 95120-6099
(Received 22 October 1987)

We present detailed results of self-consistent-field pseudopotential calculations for the stability, structural phase transitions, growth, and the electronic properties of strained Si/Ge semiconductor superlattices and alloys. The metastable structure of $(\mathrm{Si})_n/(\mathrm{Ge})_n$ ($n \leq 6$) superlattices pseudomorphically restricted to the Si(001) surface are determined through total energy minimization and interatomic force calculations, and their formation energies are calculated. A simple model for the formation energy of superlattices is developed, whereby the energy of the activation barrier to form a misfit dislocation is estimated. A neostructural phase transition in the strained Si-Ge alloy is studied, and the order of instability for various possible structures is given. It is found that during growth the atoms of the topmost grown layer are dimerized, resulting in a possible short-range order in the alloy. The energy gap of all $(\mathrm{Si})_n/(\mathrm{Ge})_n$ superlattices is found to be indirect. A more significant finding, however, is that the energy separation between the direct and indirect gap continues to decrease with increasing n, and is only 0.07 eV for $n=6$. Conduction-band states of an extended nature located below the confined states point to a new feature of the band offset and quantum-size effect. Localized states lying deep in the valence- and conduction-band continua are another novel result of this study.

I. INTRODUCTION

Its excellent etching and mechanical properties have made silicon an indispensable material in microelectronic technology. However, being an indirect-gap semiconductor, silicon has been excluded from photonics and optoelectronics. Improving electronic properties of this crystal has been the continuing interest of material scientists. Recent progress in the fabrication of epitaxial semiconductor superlattices with multiple quantum-well structure providing novel two-dimensional (2D) electronic properties has stimulated the idea of increasing carrier mobility in Si/Ge heterostructures by modulation doping. In an effort to compensate for the deficiencies of silicon, and to further upgrade this well-established technology, the epitaxial growth of the pseudomorphic $\mathrm{Si/Si_{1-x}Ge_x}$ heterostructures has been achieved.[1-5] The lattice misfit of $\leq 4\%$ is completely accommodated by the uniform lattice strain in the commensurate or pseudomorphic $\mathrm{Si/Si_{1-x}Ge_x}$ layers. While the grown layers are in registry with the epilayer, the lattice constant in the perpendicular direction expands, leading to a tetragonal distortion. This way the energy increased by the planar compressive strain is partly relieved by the perpendicular expansive strain. Owing to the high-energy barrier associated with the reordering of atoms, many defect free, strained layers can grow before the accumulated strain energy is relaxed by the generation of the misfit dislocation. Fiory *et al.*[3] were able to grow high quality, commensurate $\mathrm{Si_{1-x}Ge_x}$ films of ~ 2500 Å thickness when $x < 0.5$.

Recently, the growth of pure Ge (i.e, $x=1$) up to six layers pseudomorphically restricted to Si(001) substrate has been realized by Pearsall *et al.*[6] More importantly, they observed direct optical transitions in the $(\mathrm{Si})_4/(\mathrm{Ge})_4$ semiconductor superlattice [grown on the Si(001) substrate], which are found neither in constituent crystals nor in the $\mathrm{Si_{0.5}Ge_{0.5}}$ alloy. This has been an encouraging step towards making significant improvements in the electronic properties of silicon. Concomitantly, novel electronic structures, especially dramatic lowering of the direct gap upon superlattice formation, have been predicted by self-consistent-field pseudopotential calculations of Ciraci and Batra,[7] and Froyen, Wood, and Zunger.[8] The observed optical transitions were also investigated by using the effective-mass approximation,[9] and the tight-binding method.[10]

The stability of the Si/Ge heterostructures in spite of a large lattice mismatch is another interesting aspect. This became the focus of attention by a recent observation of Ourmazd and Bean,[11] who presented evidence for a neostructural order-disorder transition in the $\mathrm{Si(001)/Si_{1-x}Ge_x}$ strained superlattice system. Apart from its fundamental and academic relevance to the order-disorder transitions in alloys, this observation had important technological implications. The questions have arisen as to why and how the observed transition occurs, and how the long-range order affects the electronic properties of the superlattice. Theoretical studies[7,12] have started to investigate these issues. The band offset in the strained Si/Ge superlattices has attracted much attention, and is treated in a number of recent publications.[13-21] Raman spectroscopy has shown that the quantum-well structure and the band lineup are strongly dependent on the strain induced by the lattice mismatch.[15]

Clearly, the pseudomorphic Si/Ge superlattices present new conceptual ideas about synthetic semiconductors and novel device applications. A generalized formula for such a superlattice $\{\mathrm{Si_{1-x}Ge_x}\}_{n,a_\parallel}/$

 ©1988 The American Physical Society

$\{Si_{1-y}Ge_y\}_{m,a_\parallel}$ provides many degrees of freedom for controlling the electronic properties of this system. The concentration x and y of Ge in the sublattices and the lateral lattice constant $a_\parallel$ are variables, which set the band offset[15,19] and provide excellent means to engineer the quantum-well structure. The superlattice periodicity, $n+m$, (n as well as m itself) are also important parameters to control the character and the dimensionality of the confined states.[22,23] Furthermore, the modulation doping ranging from low impurity concentration to the formation of impurity bands brings about additional degrees of freedom in characterizing the devices based on these heterostructures.

In this paper we present our detailed results for the stability, neostructural phase transitions, growth, and the electronic properties of the strained $Si/Si_{0.5}Ge_{0.5}$ and $(Si)_n/(Ge)_n$ ($1 \le n \le 6$) superlattices, which have in-plane registry with the Si(001) surface. Our results are based on the total energy, force, and charge-density calculations performed by using an *ab initio* pseudopotential method. Some of our results were reported briefly elsewhere.[7] The method and the parameters of the calculations are presented in the following section. In Sec. III, the structural parameters are determined, and formation energies of superlattices are calculated. Based on these calculations the stability of $(Si)_n/(Ge)_n$ is discussed, and a simple model for obtaining the formation energy is proposed. The stability of the Si-Ge alloy, and neostructural phase transitions are treated in Sec. IV. The benefit of energy from this order-disorder transition is found to be too small. The observed phase transition may be initiated by the short-range order set up during the growth. This possibility is explored in the microstructure of the growth. This analysis is presented in Sec. V. Novel features of the electronic structure, such as the quasidirect band gap, confined states near the band edge and in the band continua, are presented in Sec. VI. Finally, our conclusions are stated in Sec. VII.

II. METHOD AND PARAMETERS OF CALCULATIONS

Self-consistent-field (SCF) pseudopotential calculations[24] were provided within the framework of the local-density functional theory applied in momentum space.[25] Scalar relativistic effects were included via the use of nonlocal, norm-conserving ionic pseudopotentials given by Bachelet *et al.*[26] Ceperley-Alder exchange and correlation potential[27] as parametrized by Perdew and Zunger[28] has been used. Bloch states are expanded with the kinetic energy cutoff corresponding to $|\mathbf{k}+\mathbf{G}|^2=12$ Ry, which leads to a basis set consisting of ~ 1200 plane waves in large unit cells. This energy cutoff is raised to 15–18 Ry to investigate the electronic structure. During the SCF iterations the valence charge density was sampled by using nine special points in the reduced zone. That this sampling is appropriate was tested by comparing total energies with those calculated with 75**k** points uniformly distributed in the tetragonal Brillouin zones (BZ). The large basis set, a fine BZ sampling, and a strict self-consistency tolerance of [root-mean-square (rms) deviation in potential] 5×10^{-7} Ry used in this study assure values for the calculated structures with acceptable accuracy. A reliable analysis for the stability of these structures relative to the constituent crystals can also be provided by comparing the calculated total energies.

We have carried out total energy, electronic structure, interatomic, and charge-density calculations on Si, Ge tetragonally distorted Ge, zinc-blende Si-Ge, and the strained $(Si)_n/(Ge)_n$ superlattices with $1 \le n \le 6$. To understand the origin of the observed neostructural phase transitions in the $Si_{1-x}Ge_x$ alloys, we also investigated the strained and also strain-free Si-Ge in the rhombohedral structure. We have determined the equilibrium structures by the method of the total energy minimization. Then, we tested these equilibrium structures by calculating the interatomic forces.[29] To obtain accurate values for interatomic forces[30] our self-consistency tolerance is reduced to $\sim 10^{-8}$ Ry.

III. ENERGETICS AND STABILITY ANALYSIS FOR $(Si)_n/(Ge)_n$ SUPERLATTICES

In this section we present results of our geometry optimization and energetics for Si, Ge, zinc-blende Si-Ge, and the strained $(Si)_n/(Ge)_n$ superlattices with $1 \le n \le 6$. All these structures are grouped according to the tetragonal unit cells in which they are treated. For example, tetragonally strained Ge, zinc-blende-SiGe, $(Si)_1/(Ge)_1$, and $(Si)_2/(Ge)_2$ are studied in tetragonal unit cells includ-

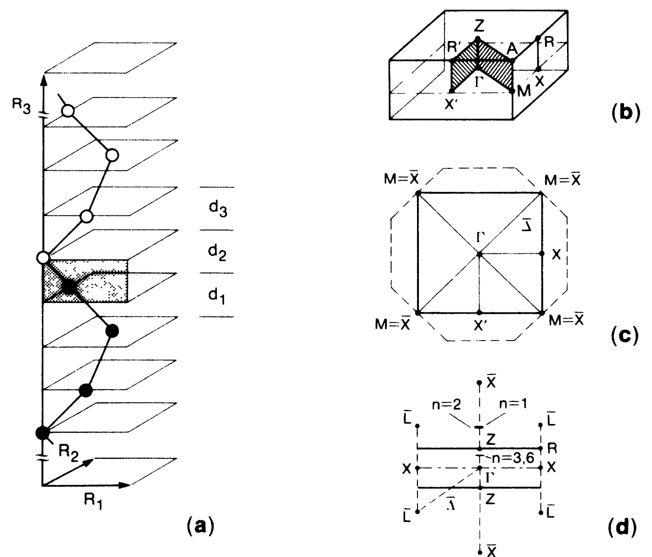

FIG. 1. (a) Tetragonal unit cell of the strained $(Si)_n/(Ge)_n$ superlattice with the solid and open circles denoting the position of Si and Ge atoms, respectively. $R_1=R_2=a^0_{Si}/\sqrt{2}$ and $d_1=a^0_{Si}/4$. R_3, d_2, and d_3 are obtained by minimization of the total energy. In all unit cells the first Si atom starting from the Si sublattice is located at the corner of the basal square of the tetragon. (b) Perspective view; (c) cross section through the horizontal central plane with dashed lines delineating the fcc BZ; (d) cross section through the vertical plane of the tetragonal superlattice Brillouin zone. The relation to the fcc BZ points labeled by the bar is indicated. ($\Gamma\bar{X}=2\pi/a^0_{Si}$ and $X\bar{L}=\pi/a^0_{Si}$.)

ing two atoms from each constituent. While $(Si)_4/(Ge)_4$ is studied in a tetragonal unit cell including four atoms from each constituent, because of their different repeat periods $(Si)_3/(Ge)_3$ and $(Si)_6/(Ge)_6$ systems are treated in a unit cell consisting of six atoms each. The tetragonal unit cell and the corresponding superlattice Brillouin zone (SBZ) is illustrated in Fig. 1. To assure commensurability in the (001) plane, the lateral lattice constants of the pseudomorphic Si/Ge superlattices $a_{\parallel}$ (in terms of cubic lattice constants) are taken to be equal to a^0_{Si}. This way a planar compressive strain $\varepsilon=(a^0_{Ge}-a_{\parallel})/a^0_{Ge}$ is introduced in the Ge sublattice.

As seen in Fig. 1 the lattice constant perpendicular to epilayers R_3 (or $a_{\perp}$ in terms of cubic lattice parameters) are determined by three types of interlayer spacings, i.e., d_1(Si—Si), d_2(Si—Ge), and d_3(Ge—Ge). The change in the value of d_1 upon superlattice formation [restricted to the Si(001) surface] is, however, negligibly small. So fixing d_1 equal to $a^0_{Si}/4$, we concentrate on the tetragonally distorted Ge sublattice. The preferential accommodation of strain by Ge layers is consistent with experimental observations,[11] and also with higher values of force constants[31] for Si relative to Ge. In the present fully relaxed calculations, d_2 is determined by the minimization of the total energy of $(Si)_1/(Ge)_1$. The determination of the perpendicular lattice constant for $(Si)_n/(Ge)_n$ with $n \geq 2$ has required the optimization of the total energy with respect to two structural degrees of freedom (i.e., optimization with respect to d_2 and d_3). Then, the values of d_2 and d_3 are obtained by the optimization of total energy through their simultaneous variation in $(Si)_2/(Ge)_2$. The value of d_2 was practically unaltered by going from $(Si)_1/(Ge)_1$ to $(Si)_2/(Ge)_2$. Eventually, these calculated values for d_1 and d_2 are used to find the perpendicular lattic constant of $(Si)_n/(Ge)_n$ with $n \geq 3$. The appropriateness of this approximation was tested by the interlayer force calculations. As seen in Fig. 2, calculated forces for $(Si)_4/(Ge)_4$ vary in the range of 10^{-2}–10^{-3} mdyn (or 10^{-10}–10^{-11} N), and thus confirm that—within the accuracy of our calculations—d_2 and d_3 remain

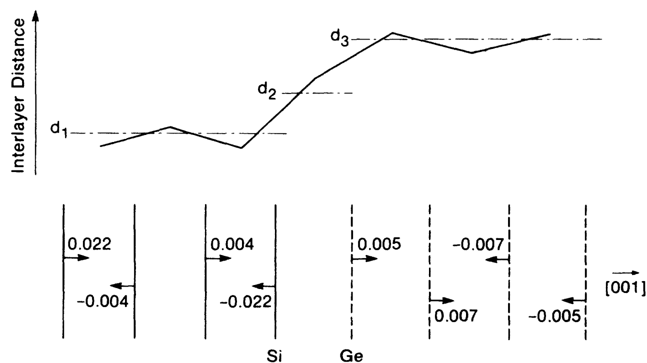

FIG. 2. Calculated interlayer forces for the structure optimized, pseudomorphic $(Si)_4/(Ge)_4$ superlattice with the SCF tolerance (rms deviation in potential) of 10^{-8} Ry. The unit of force is mdyn/atom (1 mdyn$=10^{-8}$ N). Based on the force values the small variation of the interlayer spacings are shown systematically.

nearly unaltered in a superlattice with a larger repeat distance. However, an interesting feature one deduces from this figure is that Ge—Ge spacing near the interface has to be slightly larger than that near the middle of the Ge sublattice. In contrast to this, the Si—Si spacing at the center of the Si sublattice is larger than that adjacent to the interface. These small variations of the interlayer spacings suggest that vertical strains are not uniformly distributed over the layers. Nevertheless, these variations are very small in the present geometry, and thus are neglected.

Calculated equilibrium values for the interlayer spacings are $d_1=2.56$ a.u., $d_2=2.61$ a.u., and $d_3=2.70$ a.u. It should be noted that the calculated d_2 is very close to the average value for Si and Ge, i.e., $(a^0_{Si}+a^0_{Ge})/8$; whereas the value of d_3 implies a tetragonal distortion, $\varepsilon_T=(a_{\perp}-a_{\parallel})/a^0_{Ge}$ of $\sim 5\%$ in the Ge sublattice. For Ge epitaxially restricted to Si(001), i.e., $a_{\parallel}=a^0_{Si}$ and denoted as Ge^{ep}, the interlayer spacing $a_{\perp}/4$ is found to be nearly equal to d_3. For the sake of comparison, the equilibrium structure of zinc-blende SiGe is also determined in the tetragonal unit cell by maintaining the cubic symmetry. The calculated equilibrium lattice constant is $a^0_{\text{zinc-blende SiGe}}=10.40$ a.u.

In order to provide a consistent comparison of the energetics for the stability analysis, the total energy differences were calculated by using the same number of atoms and similar unit cells. For example, the formation energy (or formation enthalpy at $T=0$) of the pseudomorphic $(Si)_n/(Ge)_n$ superlattice is calculated,

$$\Delta E^{f,s}((Si)_n/(Ge)_n)=E^s_T((Si)_n/(Ge)_n) - [E^0_T((Si)_{2n})+E^0_T((Ge)_{2n})]/2 ,$$

where the total energies of the constituent strain-free crystals $E^0_T((Si)_{2n})$ and $E^0_T((Ge)_{2n})$ are calculated in a unit cell corresponding to that of $(Si)_n/(Ge)_n$, but with the equilibrium lattice constants (a^0_{Si} and a^0_{Ge}) determined for the (strain-free) bulk crystals. So the total energies of Si and Ge with the bulk equilibrium lattice constants have been calculated for the tetragonal unit cells containing 4, 8, and 12 atoms. The formation energy of the (strain-free) zinc-blende SiGe is defined as

$$\Delta E^{f,0}(\text{zinc-blende SiGe})=E^0(\text{zinc-blende SiGe}) - [E^0(\text{Si})+E^0(\text{Ge})]/2 ,$$

and calculated to be ~ 1.05 mRy per atom pair. This is 0.27 mRy smaller than the value reported by Martins and Zunger.[12] The calculated formation energies of the strained superlattices are given in Table I, wherefrom we draw the following conclusions. (i) All superlattice formation energies have positive values. By definition, the formation energy $\Delta E^{f,s}>0$ indicates instability. Consequently, the decomposition into constituent crystals (i.e., segregation) is favored, as long as permitted by the kinetics of the reaction. Alternatively, the strain energy accumulated in the Ge sublattice can be relieved by the creation of a misfit dislocation (or by other types of defects). (ii) The value of $\Delta E^{f,s}$ increases with increasing n because the Ge sublattice has more strained layers. Also

TABLE I. Calculated formation energies of the pseudomorphic $(Si)_n/(Ge)_n$ superlattices. The unit of energy is mRy per $(Si)_n/(Ge)_n$ unit.

$n=1$	$n=2$	$n=3$	$n=4$	$n=6$
1.46	1.73	5.04	7.03	9.29

for large n, $\Delta E^{f,s}/n$ saturates to a constant value. This is different from what we find for the lattice matched superlattices. For example, in $(GaAs)_n/(AlAs)_n$ in the [001] orientation, $\Delta E^f/n$ was found[23] to be inversely proportional to n. This is a natural consequence of the fact that in the lattice matched superlattices, ΔE^f is equal to the interfacial energy, and the strain energy has practically no contribution. (iii) Although $(Si)_6/(Ge)_6$ and two formula units $(Si)_3/(Ge)_3$ have the same number of atoms in their unit cell, the former has smaller $\Delta E^{f,s}$ than twice the $(Si)_3/(Ge)_3$ formation energy. The same is true for $(Si)_1/(Ge)_1$ and $(Si)_2/(Ge)_2$. This indicates the significant contribution of the interfacial energy in $\Delta E^{f,s}$. However, the above trend seems to be invalid between $(Si)_2/(Ge)_2$ and $(Si)_4/(Ge)_4$. Since for $n=2$ the bulk potentials in the sublattices are not fully developed, $\Delta E^{f,s}((Si)_2/(Ge)_2)$ should not be compared directly with $\Delta E^{f,s}((Si)_4/(Ge)_4)$.

The above conclusions suggest that the formation energy of the superlattices with $n>2$ has two major components. These are interfacial energy and the strain energy. If the transfer of charge from one sublattice to the other is confined in a narrow region near the interface (and thus the resulting redistribution of charge in the sublattice is insignificant), these two components of the formation energy $\Delta E^{f,s}$ can be dealt with separately. The interfacial energy is related to the heteropolar (Si—Ge) bond formation and charge rearrangements across the interface. The strain, on the other hand, changes the equilibrium structure and the charge distribution in the Ge sublattice. Redistribution of charge is the primary cause of the (positive) strain energy. Using the planarly averaged charge density we were able to calculate the amount of charge between the two planes parallel to the epilayer. The charge between any two adjacent atomic planes is found to be 4 ∓ 0.02 electrons per surface unit cell. The deviations from the valency of constituent atoms are within the accuracy of our scheme for integrating charge density. This analysis shows that the transfer of charge from one sublattice to the other is negligibly small for $(Si)_n/(Ge)_n$, which is consistent with the electronegativity arguments. Calculated total (valence) charge densities in Fig. 3 indicate that the charge of the heteropolar Si—Ge bond is simply the combination of the homopolar bonds[12] (i.e., it is asymmetric, and Ge-like near the Ge atom, and Si-like near the Si atom). The effect of the tetragonal strain in the epitaxial Ge lattice is to increase the bond charge in Fig. 3(b). Then the charge distribution at the interface of a superlattice in Fig. 3(c) is seen to be a combination of the charge of Si and epitaxial Ge. The charge between Si and Ge interface layers is found to be ~4 electrons per unit cell. Contour plots of the total

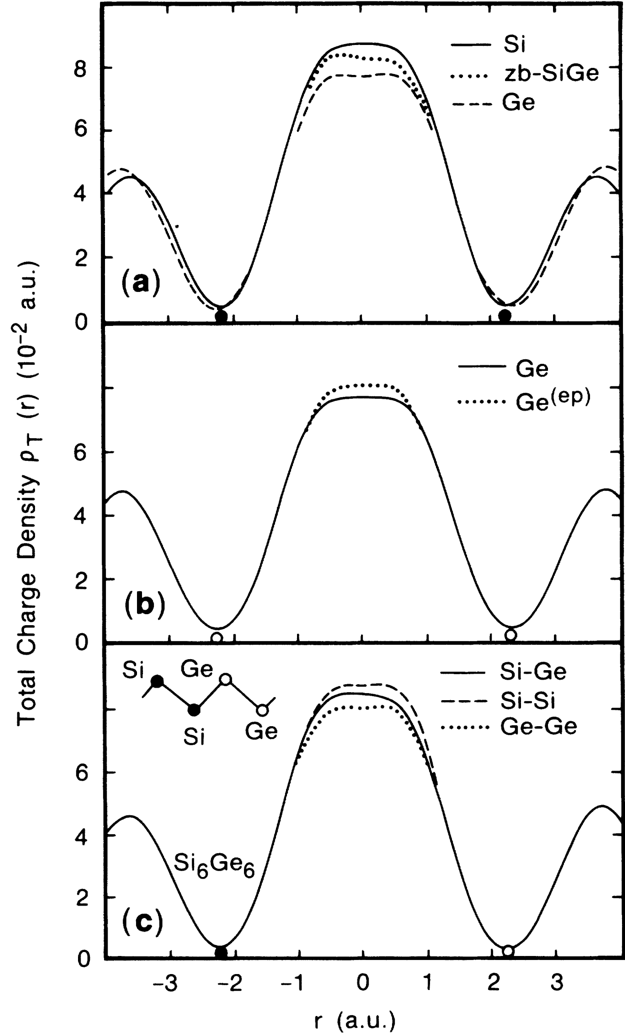

FIG. 3. Distribution of valence charge calculated along the bond. (a) Unstrained Si, Ge, and zinc-blende SiGe; (b) unstrained Ge and epitaxial Ge [restricted to the Si(001) surface]; (c) interface of $(Si)_6/(Ge)_6$, and adjacent Si—Si and Ge—Ge bonds. The unit for charge density in a.u. is e/bohr^3.

charge density illustrated in Fig. 4 suggest that the interface and the bulk regions (Si and Ge^{ep}) are distinguished, and the character of the interface is indeed unaltered for $n\geq3$. In view of the above analysis we now develop a simple model to obtain $\Delta E^{f,s}$. To this end, we imagine the formation of the superlattice in three steps. First, we impose a tetragonal distortion along the [001] direction in Ge, and thus introduce the strain energy in the Ge lattice. The strain energy per atom in the Ge sublattice is defined as

$$\xi=[E_T^s((Ge)_n)-E_T^0((Ge)_n)]/n ,$$

in terms of the energy, $E_T^s((Ge)_n)$ of the epitaxial Ge^{ep} calculated in a tetragonal unit cell containing n atoms. It is found to be $\xi=1.46$ mRy per epitaxial Ge atom. Clearly, one could have estimated this number from known elastic constants for Ge. However, for internal

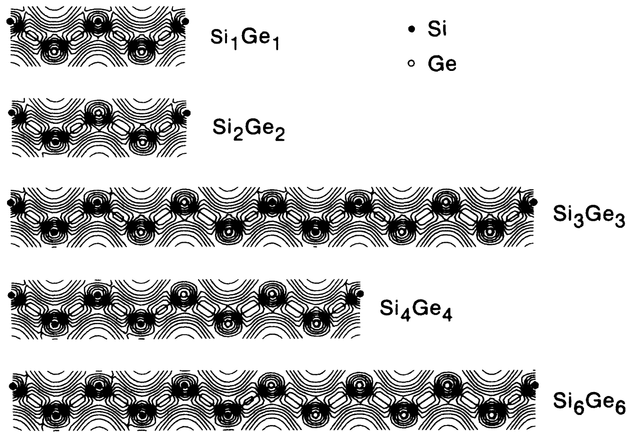

FIG. 4. Contour plots of the valence charge densities for $(\mathrm{Si})_n/(\mathrm{Ge})_n$ superlattices. Si and Ge atoms are shown by solid and open circles, respectively. Contour spacings are 0.009 e/bohr^3.

consistency we have chosen to calculate this value from the self-consistent calculations. In the second step, we create n Si(001) and n Ge(001) slabs in registry, by breaking homopolar Si—Si and Ge—Ge bonds. In the third step, we make Si/Ge interface by forming the heteropolar Si—Ge bonds. The last step requires the interfacial energy, which is approximately equal to the difference of energy between the heteropolar and homopolar average. By using the calculated $\Delta E^{f,0}$ (zinc-blende SiGe) we estimate the interfacial energy, $\chi = \Delta E^{f,0}$ (zinc-blende SiGe)/2, to be ~ 0.5 mRy per atom. Then, the superlattice formation energy is defined as

$$\Delta E^{f,s}((\mathrm{Si})_n/(\mathrm{Ge})_n) \simeq 2\chi + n\xi \; .$$

In Fig. 5 the formation energies estimated from this simple model are compared with our *ab initio* results,

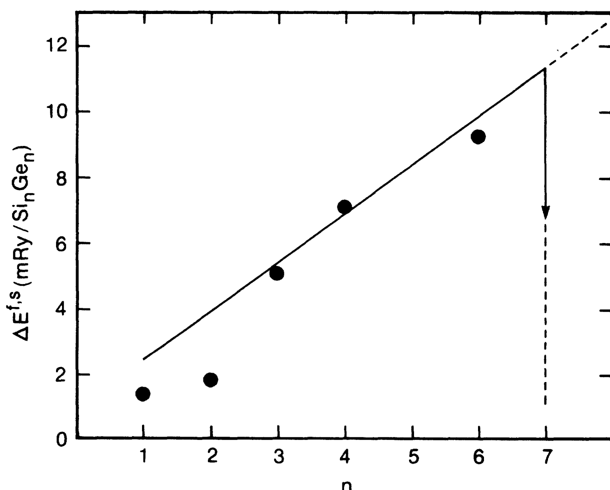

FIG. 5. Comparison of the calculated formation energies (solid circles) with those estimated from a simple linear relation developed in the text. The width of Si and Ge sublattices is n.

displaying an almost perfect match for $n \geq 3$. Owing to the small superlattice periodicity, $(\mathrm{Si})_1/(\mathrm{Ge})_1$ (epitaxial zinc-blende SiGe) and $(\mathrm{Si})_2/(\mathrm{Ge})_2$ deviate from this simple model. The above model can be further improved to include structures with $n=1$ and $n=2$. The strained Ge layers adjacent to the interface are distinguished from those lying near the center, and thus two types of strain energy are defined. The strain energy for the layers adjacent to the interface are estimated from $\Delta E^{f,s}((\mathrm{Si})_1/(\mathrm{Ge})_1)$. Within this simple approach, the formation energy of $(\mathrm{Si})_7/(\mathrm{Ge})_7$ is predicted to be ~ 11.3 mRy. As revealed from earlier experimental work,[6] only six epitaxial Ge layers can grow on Si(001), and beyond that thickness misfit dislocations are generated. The above model thus yields an estimate for the formation-energy barrier to form a misfit dislocation to be $9.8 < \Delta Q < 11.3$ mRy/cell.

IV. PHASE TRANSITIONS IN Si-Ge ALLOYS

Having discussed the stability of superlattices, we next consider the stability issues related to Si-Ge alloy, which has also positive energy of formation ($\Delta E^{f,s} > 0$). Therefore, a phase transition to a different structure, or decomposition into constituent crystals (i.e., segregation) is expected. Such a segregation has not been observed so far, due perhaps to the relatively small kinetic energy of atoms to overcome the activation barrier at low temperature. This situation at low temperature, however, may be different beyond some critical temperature T_c where the Si-Ge alloy may be stabilized by the entropy of disorder.

Since the neostructural phase transition is observed[11] in the Si-Ge alloy grown on the Si(001) surface, its origin has to be sought in the strain energy introduced by the lattice mismatch. Ourmazd and Bean[11] proposed two variants for the ordered phase, both being in the rhombohedral structure. These structures can be viewed as the bilayer segregation along the offset [111] direction in the strained Si-Ge alloy. In the first structure, denoted RS1, Si(Ge) has three heteropolar (i.e., Si—Ge) and one homopolar bond (i.e., Si—Si or Ge—Ge). The widely spaced planes along the [111] direction are formed by atoms of the same kind. In the second structure, RS2, Si(Ge) has one heteropolar, and three homopolar bonds, and pairs of widely spaced planes are formed by atoms of the opposite kind (see Fig. 6).

To find the cause of the neostructural phase transition in the strained $\mathrm{Si}_{0.5}\mathrm{Ge}_{0.5}$ alloy we proceed by comparing the total energy of the alloy with other ordered structures including those of the constituent Si and Ge crystals. This has, however, two crucial aspects. One is the well-known convergence problem with respect to the size of the plane-wave basis set used in the calculation of the total energy. The absolute convergence in total energies requires very large basis sets, which cannot be handled easily for supercells. Not being able to achieve this, a realistic comparison can be provided, however, among the total energies nearly converged, but calculated for the unit cell having the same Bravais lattice symmetry, and comprising of the same number of atoms. Secondly, since the proposed ordered structures are not in the equilibri-

um state, but are distorted under the lattice strain, their structural parameters (i.e., the interlayer spacings, and atomic positions in the cell, etc.) have to be consistent with the observed strain.[5] The supercell shown in Fig. 6, which contains eight Si and eight Ge atoms, satisfies these constraints. In addition it is expedient for the study of the totally segregated $(Si)_4/(Ge)_4$ system, the epitaxial zinc-blende SiGe, and to some extent also the "quasi" disordered $Si_{0.5}Ge_{0.5}$ alloy.

The disorder in the $Si_{0.5}Ge_{0.5}$ alloy is simulated by our creating supercells with altered coordination sequence of atoms and averaging the total energies. As discussed in Sec. III, the strain is introduced by the use of a^0_{Si} for the lattice parameters parallel to the epilayer in all supercells. The spacing between Si and the strained Ge(001) layer, and the spacing of adjacent Ge layers are obtained by total-energy minimization. The spacing of the $Si_{0.5}Ge_{0.5}$ layers is obtained by scaling the x-ray-measured vertical (expansive) strain[3] with respect to the calculated equilibrium lattice constants. The work by Van de Walle and Martin[19] has justified this approach.

Our total energy calculations yield that the strained RS1 structure has slightly lower energy (1 mRy/cell) relative to the "averaged" disordered structure representing $Si_{0.5}/Ge_{0.5}$ alloy. This explains why the order-disorder transition can occur. The equilibrium structure of the strain-free RS1 is optimized in the primitive (four-atom) unit cell. The calculated total energy is found to be 0.75 mRy (atom pair) higher than the average of the bulk Si and Ge in their equilibrium structure. According to this result, the ordered, strain-free RS1 structure is stable relative to the strained alloy, but is unstable relative to the decomposition into Si and Ge. It becomes even more unstable under the strain introduced by lateral epitaxy. Since we find the total energy of the ordered phase RS2 to be higher than that of RS1 (both being under the strain of the lattice), we conclude that RS2 is unfavorable as far as the order-disorder transition is concerned. An important result we find is that forming a strained $(Si)_4/(Ge)_4$ superlattice as described in Fig. 6(d) is even more favorable than the strained RS1 phase, with an energy benefit of ~ 0.5 mRy (atom pair). The degree of instability of these phases in terms of their formation energies relative to the average energy of equilibrium Si and Ge is ordered as

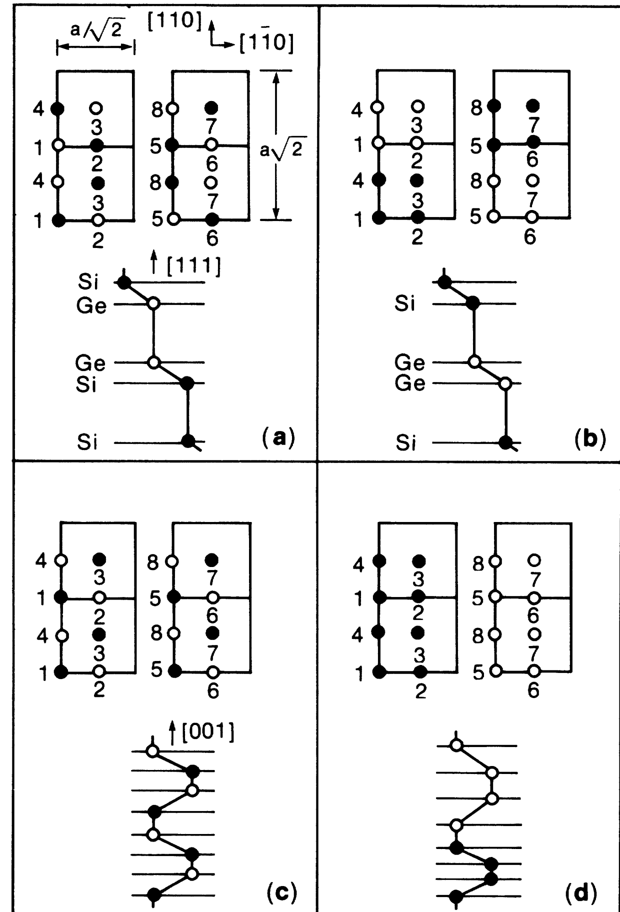

FIG. 6. The unit cell consisting of eight (001)-(2×1) layers with eight Si and eight Ge atoms used in the stability analysis of the Si-Ge alloy. Numerals identify the layers. For clarity, the first and second sets of four layers are shown separately. (a) Strained rhombohedral structure RS1; (b) strained RS2; (c) strained zinc-blende SiGe; and (d) segregated structures. The ordering of layers is shown along the offset [111] direction (for RS1 and RS2), and along the [001] direction (for zinc-blende and segregated structures).

$$\Delta E^{f,s}(Si_{0.5}Ge_{0.5}) > \Delta E^{f,s}(RS2) > \Delta E^{f,s}(\text{zinc-blende SiGe}) > \Delta E^{f,s}(RS1) > \Delta E^{f,s}((Si)_4/(Ge)_4) > \Delta E^{f,0}(RS1) > 0 .$$

Martins and Zunger[12] have studied the stability of the epitaxial RS1 phase relative to the epitaxial zinc-blende SiGe and the average of Si and epitaxial Ge. The formation energies they calculated for the strain-free zinc-blende SiGe and RS1 are in fair agreement with the present results. They found the strained RS1 has lower energy relative to the average energy of Si and epitaxial Ge. Our result $\Delta E^{f,s}(RS1) > \Delta E^{f,s}((Si)_4/(Ge)_4)$, however, indicates the epitaxial RS1 phase considered in Fig. 6(a) has higher lattice strain. Accordingly, the experimental observation that the ordering is reduced during prolonged annealing may be due to the onset of segregation.

V. GROWTH OF Ge ON A Si(001) SURFACE

From the above discussion it emerges that the ordered RS1 structure is favorable relative to the alloy. However, the benefit of energy is found to be too small to induce such a phase transition. To understand the origin of this

dilemma, we focus our attention on the microscopic aspects of the growth process on the Si(001) substrate. Assuming a layer-by-layer growth of the adatoms (Si or Ge), the important question we explore is the atomic structure of the topmost grown layer. This has relevance to the quality of the heterostructures and to the phase transitions, as well.

Several studies[32,33] in the past decade have established that the free Si(001) surface undergoes a (2×1) reconstruction. Two surface atoms in the adjacent cells, each having two dangling bonds, are tilted so that an interaction between them leads to a dimer bond (σ), and an antibonding bond (σ^*). Remaining dangling bonds, one at each surface atom, form π and π^* surface states in the gap. Since the benefit of energy by forming the dimer bond is much larger than the energy lost through lattice distortion, the (2×1) reconstruction is stable by an energy gain[33] of ~ 0.75 eV per surface Si. Recent studies[33-35] have indicated also extended defects (missing rows etc.), which enhance the stability of the dimer structure. Since the grown Si layers are strain free, the same atomic configuration is expected to occur in the topmost grown Si layer. Accordingly, the last Si layer has to grow subsequent to the breaking of dimer bonds in the subsurface layer, but it itself forms dimer bonds eventually. Since the dimer bonds are broken upon the growth of a new layer, the extended defects may also be removed under normal growth conditions.

A similar (2×1) reconstruction together with local $c(2\times2)$ and $p(4\times2)$ symmetry has been observed on the Ge(001) surfaces.[36] Consequently, the dimer bond is also the essential feature of this surface. Owing to the lattice strain, the situation, whether the dimer bond does occur in the pseudomorphic Ge layers grown on the Si(001) surface, is not so obvious. The structure of the topmost grown Ge layer is explored by the total energy calculations. We have optimized the position of Ge atoms adsorbed on the Si(001) surface as if they continue the bulk structure. The geometry optimization gave the Si-Ge interlayer distance close to that of the average of Si and unstrained Ge. This has also been found earlier by Batra[37] for Al adsorbed on the Ge(001) surface. In the second step, the (2×1) reconstruction geometry with the Ge—Ge dimer bonds above the Si surface is constructed. The total energy of this reconstructed surface is found to be ~ 0.5 eV (per surface Ge atom) lower than that of the ideal structure. This clearly indicates that the ideal structure undergoes a reconstruction, and may form dimer bonds (if there is no other structure with even lower energy). Unfortunately, the extended defects cannot be considered by the present method. Following the above arguments, it is anticipated that each Ge layer grows by breaking the existing dimer bonds, and forming new ones in the latest grown layer.

In view of the energetics, the reconstruction becomes important in the growth of the $Si_{1-x}Ge_x$ layer. Since Si—Si and Ge—Ge dimer bonds form, the Si—Ge dimer bond can also form. However, as found in the previous section, the Si—Ge heteropolar bond is energetically unfavorable as compared to the homopolar average, implying a preferential adsorption and a selective dimerization. Also note that upon Si—Si dimerization ~ 0.5 eV more energy is released as compared to the Ge—Ge dimerization. The selective dimerization, on the other hand, is expected to induce short-range order, or domain structure in each grown layer. As seen in Fig. 6, the ordered RS1 structure can be easily constructed by short-ranged rearrangements of Si and Ge in the grown layer. Taking the high mobility (and thus sizeable kinetic energy) of the adatoms during the growth, this seems to be likely.

VI. ELECTRONIC STRUCTURE

It is known that the SCF pseudopotential method within the local-density approach is suitable for ground-state properties, but underestimates the conduction-band energies, and thus yields smaller band gaps. This shortcoming of the theory may lead to serious difficulties in heterostructures if the errors in the conduction-band energies of the sublattices are different. As pointed out earlier[19] this is fortunately not the case for the Si/Ge system (provided the Bloch states are represented by an appropriate number of plane waves). In Table II we compare the calculated conduction-band energies with the experimental values.[38,39] It is seen that after the spin-orbit splitting is taken into account, the average error in the conduction-band energies relevant to our study ($\bar{L}$, $\bar{X}$, and $\bar{\Delta}_{min}$ points of the fcc BZ) is ~ 0.5 eV. As a result the present study can reliably be extended to explore the electronic structure by applying a constant upward shift of 0.5 eV to the conduction-band energies. In such a scheme the error bar in the calculated-band energies is estimated to be ∓ 0.05 eV.

A. Band structure

Silicon substrate has six minima along the $\bar{\Delta}$ directions of the fcc BZ, $\bar{\Delta}_{min}$ (with transverse effective mass $m_t^* = 0.19 m_0$, and longitudinal effective mass $m_l^* = 0.98 m_0$), which give rise to an indirect band gap of ~ 1.1 eV. The direct band gap is large, and the energy difference between the direct and indirect band gap, $\delta E_g = E_g^{(d)} - E_g^{(i)}$, is 2.3 eV. Germanium is also an indirect band-gap semiconductor, except that the

TABLE II. Experimental and calculated values (in eV) of the selected conduction-band states relative to the maximum of the valence band. E_x denotes experimental values obtained from Refs. 38 and 39. E_L and E_H are band energies calculated with cutoffs $|\mathbf{k}+\mathbf{G}|^2$ of 12 and 15 Ry, respectively. $\Delta E_{L(H)} = E_x - E_{L(H)}$.

	E_x	E_L	ΔE_L	E_H	ΔE_H
		Silicon			
$\bar{\Gamma}_{15'}$	3.37	2.56	0.81	2.56	0.81
$\bar{X}_1$	1.30	0.67	0.63	0.65	0.65
$\bar{L}_1$	2.10	1.62	0.48	1.51	0.59
$\bar{\Delta}_{min}$	1.11	0.52	0.59	0.51	0.60
		Germanium			
$\bar{\Gamma}_{2'}$	0.89	0.69	0.20	0.36	0.53
$\bar{X}_1$	1.30	0.69	0.61	0.69	0.61
$\bar{L}_1$	0.74	0.39	0.35	0.29	0.45

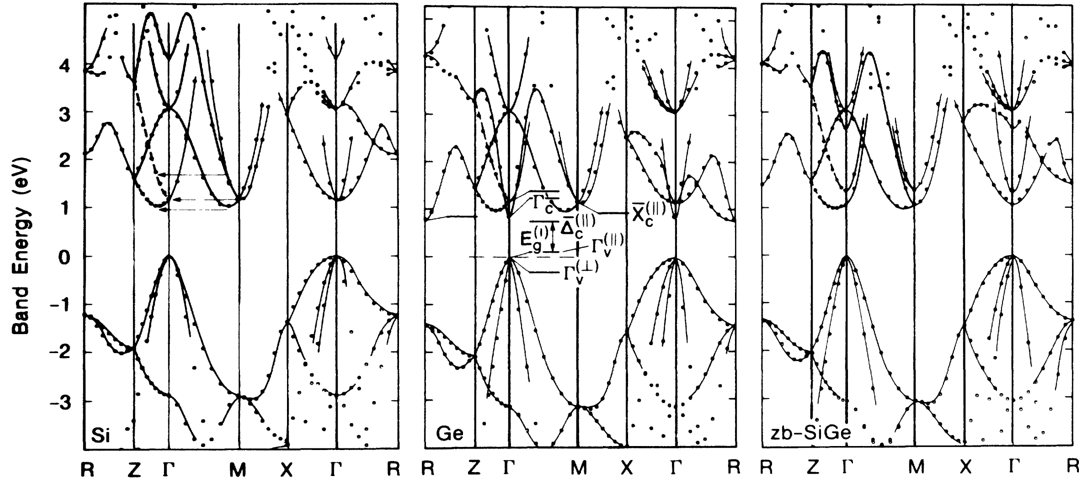

FIG. 7. Energy-band structure of $(Si)_4$, $(Ge)_4$, and zinc-blende SiGe calculated in the tetragonal unit cell. Folded bands are shown by dashed lines. Splitting and shifts of major states of tetragonally strained $(Ge)_4$ are denoted by bars. The zero of energy is set to the maximum of the valence band.

conduction-band minima occur at the eight $\bar{L}$ points. Superlattice formation has three major effects on the electronic structure. These are zone folding[40] owing to the symmetry lowering along the superlattice direction, the strain in the Ge sublattice, and the band lineup. First we consider the effect of the zone folding. Once the O_h symmetry of the diamond structure is broken by the superlattice formation, say along the [001] direction, the bands with $\mathbf{k}\|[001]$ are folded along the ΓZ direction of the superlattice BZ (see Fig. 1). In general the zone folding along [001] lowers δE_g in Si, but has no effect on Ge (since in the conduction band of Ge, $E_{X_1} > E_{\Gamma_{2'}}$) because the minimum gap is at L. This effect is described in Fig. 7(a), where the energy bands of Si in a lower symmetry (i.e., calculated for Si_4 in the tetragonal cell) are presented. In this symmetry four M points of the SBZ are equivalent to four $(k_{\|})$ $\bar{X}$ points of the fcc BZ lying in the (001) plane. The remaining two $(k_{\perp})$ $\bar{X}$ along [001] are folded to Γ. Eight R points are also equivalent to eight $\bar{L}$ points. However, upon the breaking of the fourfold rotary-inversion symmetry, S_4, R points are separated into two groups, R and R', in a superlattice. Similarly, bands along $\bar{\Delta}$ experience a single zone folding, and occur along the ΓZ direction. As a consequence, δE_g becomes equal to the difference of energy, $E_{\bar{X}_1} - E_{\bar{\Delta}_{\min}}$. Increasing the superlattice periodicity n increases the number of folding. For example, while $(Si)_4$ has single folding, bands in $(Si)_8$ experience double folding, and $\bar{L} \rightarrow X$. However, it should be noted that in the $(Si)_n$ superlattice the folded, lowest conduction-band state cannot be lower than the minimum indirect band gap. Similar band foldings are seen for $(Ge)_4$ in Fig. 7(b). In Fig. 7(c) the electronic structure of zinc-blende SiGe in the same tetragonal cell is considered to evolve from those of $(Si)_4$ and $(Ge)_4$. At the Γ point, the folded bands are split, and the third conduction band at ~ 2.6 eV is evolved from $\Gamma_{2'}$ of Si and Ge. Because of two different (001) planes (Si and Ge), the fourfold degenerate states at M also split. These folding arguments presented for one type of sublattice will guide us in understanding the electronic structure of the superlattice heterostructure $(Si)_n/(Ge)_n$ comprised of two different sublattices.

The effect of the epitaxial (tetragonal) strain on the electronic structure of Ge is shown in Fig. 7(b). The threefold degenerate $\Gamma_{25'}$ states (in the absence of the spin-orbit coupling) at the top of the valence band are split by 0.41 eV. The deformation potential calculated from this splitting is -2.78 eV, in good agreement with the experimental value[41] -2.86 ± 0.15 eV. In addition to the strain splitting, the spin-orbit coupling[19] raises the maximum of the valence band relative to the average energy by 0.1 eV. In the conduction band, the states at the R point ($\bar{L}$), and $\Gamma_{c,1}$ (or $\bar{\Gamma}_{2'}$) and the doubly degenerate folded states, $\Gamma_{c,2\text{-}3}$ (or $\bar{X}_{c,1}$ with $k_{\perp}$) are raised, whereas the conduction-band states at M (or $\bar{X}_{c,1}$ with $k_{\|}$) and $\bar{\Delta}_{\min}$ are lowered. As seen in Fig. 7(b) the net effect is that the minimum of the conduction band changed from R to $\bar{\Delta}_{\min}$, and the direct band gap is reduced.

The third effect, i.e., superlattice formation, combines the previous effects with the band alignment. The energy of the valence-band maximum relative to the average crystal potential changes in going from one sublattice to the next one. This difference is one of the primary factors which set the band discontinuity. Normally, to attain a common Fermi level, charge is transferred from one sublattice to the next one, if their Fermi energies are different. Charge transfer (due also to different electronegativities of atoms at the interface) shifts the average crystal potentials. Eventually, bands are aligned to yield a common Fermi level and a minimum total energy for the given heterostructure (although it can be a metastable structure, and thus the system may undergo a structural change). Certainly, the band alignment is a macroscopic concept,[22,23] and is conceivable only for large superlattice periodicities, for which the effective-mass approximation

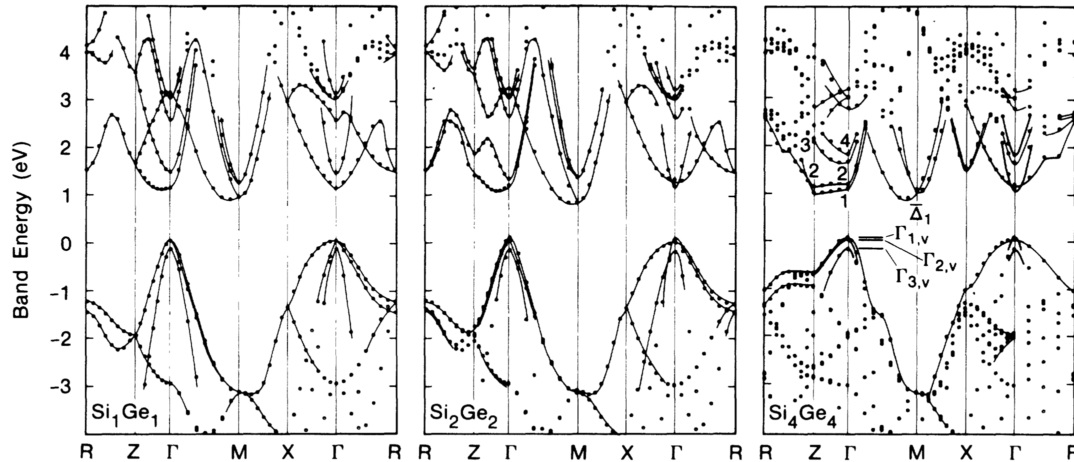

FIG. 8. Energy-band structure of $(Si)_n/(Ge)_n$ superlattices for $n=1$, 2, and 4. The zero of energy is set to the average energy of the topmost three valence-band states.

is perhaps applicable at the band minima.[42–44] By performing SCF calculations on the optimized structures, all these effects are taken into account, and the band lineup is obtained directly. Nevertheless, the superlattice effect for $(Si)_n/(Ge)_n$ $(3\leq n\leq 6)$ can be deduced by shifting[9] the bands of $(Ge)_n$ relative to $(Si)_n$ by the offset of the valence bands.

To establish a connection between the calculated band structure and quantum-well states, we consider two sublattices separately. A state in one sublattice, $\Psi(E,k_\parallel)$, can match to the state in the other sublattice, $\Phi(E',k'_\parallel)$, as long as their momentums and energies are conserved. If $V_0=E-E'$ differs from zero near a band minimum in the $k_\parallel$ plane, the higher-energy state will be a barrier for the lower-energy state. Then the lower-energy state may be confined in its sublattice, forming a subband,

$$E(k_\parallel,k_\perp)=(m_0/m_\parallel^*)k_\parallel^2+\varepsilon(k_\perp)\ ,$$

in this new quantum regime. In a single quantum well with the large barrier sublattices on both sides, one gets at least one confined state, whose energy depends on V_0, $m_\perp^*/m_0$, and the width of the well. In a multiple, periodic quantum well generated from a superlattice, subbands, in a sense, are extended states. Bound solutions yield states localized in one sublattice. The energy of these bound states is also a function of V_0, the width of sublattice n, and $(m_\perp^*/m_0)$. The smaller are n and $(m_\perp^*/m_0)$, the higher is $\varepsilon(k_\perp)$. This is a size effect, or a quantum size effect.[41–44] The dispersion of $\varepsilon(k_\perp)$ is in general small, and is a measure of the coupling between sublattices.[44] For large superlattice periodicity (i.e., large n), localized bound states turn into the confined states, much like a metal-insulator transition. With a proper account of hole energy and effective mass, the same discussion can also be applied for the hole states. Away from the band minimum, Ψ and Φ states can form bonding and antibonding combinations if their energies do not differ significantly. Their splitting will depend on their charge distribution in the cell. Since the bond arrangement still follows the broken S_4 symmetry, the superlattice periodicities which are not divisible by 4 result in large splittings.[8] If $V_0=E-E'$ is large, they can also be localized individually in the sublattice. Such a situation may arise, for example, when one of the states has energy falling in the stomach gap of the other sublattice. We emphasize again that this simple description of the electronic structure does not persist for ultrasmall superlattice periodicities. As a matter of fact, the structures with ultrathin sublattice alterations cannot even be considered as a multiple quantum-well structure, but more appropriately a new crystal. As will be seen, $(Si)_1/(Ge)_1$ is such a crystal. But $(Si)_2/(Ge)_2$ is at the border line. We get clear quantum-well structure only for $n>3$.

We now examine the calculated electronic structure. In Fig. 8 the band structures for $n=1$, 2, and 4 show how the superlattice energy structure evolves with increasing n. To guide the eye, bands of important states are joined without a complete analysis of the band crossings. As expected, the electronic structure of $(Si)_1/(Ge)_1$ is only a slightly modified form of that of the zinc-blende SiGe. The threefold-degenerate bands at the maximum of the valence band are split due to the tetragonal strain. Apparently, the $n=1$ structure does not provide any quantum-well structure with localized states. In $(Si)_2/(Ge)_2$ the superlattice features start to appear along the ΓZ direction, where the first and second conduction-band states are separated from the extended-state bands, and have relatively small dispersion. As will be seen shortly, the $n=2$ structure provides features which go beyond the trends obtained in the others. For example, among the structures we studied here $(1\leq n\leq 6)$, $(Si)_2/(Ge)_2$ has the lowest indirect gap and largest δE_g. Moreover, the minimum of the conduction band occurs at M, and not in Δ. It has also relatively smaller superlattice formation energy. The band structure of $(Si)_4/(Ge)_4$ presented in Fig. 8(c) clearly shows that the quantum-well structure has set in. The two lowest folded bands with $\mathbf{k}_\perp$ (parallel to the superlattice direction) are flattened out, and form the subband structure. The disper-

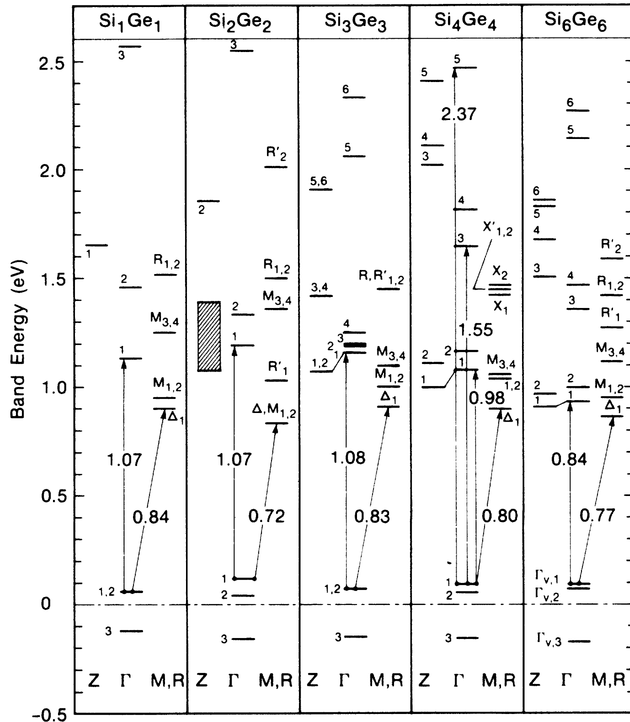

FIG. 9. Energy-level diagram of valence- and conduction-band states of $(Si)_n/(Ge)_n$ at major symmetry points. The direct ($\Gamma_{v,1} \rightarrow \Gamma_{c,1}$) and indirect ($\Gamma_{v,1} \rightarrow \Delta_{c,1}$) band gaps, and some direct transitions are indicated by arrows. The dispersion of the first conduction band of $(Si)_2/(Ge)_2$ along ΓZ is shown by the cross-hatched area.

sion of the third and fourth bands are significantly reduced. At the center of the SBZ, and in the plane parallel to the epilayer, these bands have a parabolic dispersion (i.e., $E \simeq k_{\parallel}^2$). This is the well-known behavior of the confined states with 2D character. Another interesting aspect of this superlattice is that the states deep in the valence and conduction bands are localized in certain regions of the SBZ. We consider these states as localized or resonance states, because they cannot find a matching partner.

The states of $(Si)_n/(Ge)_n$ structures relevant to our discussion are presented in an energy-level diagram shown in Fig. 9. For $n \geq 2$, the energy of the lowest conduction-band states at Γ, $E_g^{(d)}$, decreases gradually with increasing n. The dispersion (width) of the corresponding band in ΓZ also decreases with the increasing superlattice periodicity. It is 0.3 eV for $n=2$, but becomes only 0.026 eV for $n=6$. Whereas the same band in $(Si)_1/(Ge)_1$ has large dispersion. The energy of the lowest conduction-band state, which occurs along ΓM, decreases also by going from $(Si)_3/(Ge)_3$ to $(Si)_6/(Ge)_6$, but at a relatively smaller rate. This behavior is partly related to the splitting of the states at the M point of the SBZ due to the S_4 symmetry breaking along the [001] direction. The splitting of states at M is smallest for $n=4$ and largest for $n=2$, but the average energy is nearly constant. The splitting of the highest valence-band states, as well as the conduction-band states at R (or X for $n=4$) also exhibit the same trend, $(Si)_2/(Ge)_2$ always having the maximum splitting value. The difference of energy between the Δ_{min} and $M_{1,2}$ states varies with n, and decreases in going from $n=4$ to $n=6$. Since the splitting at M is expected to be small for $n=8$ (and the ΓZ dispersion is also negligibly small), the $(Si)_8/(Ge)_8$ superlattice is likely to have a zero energy difference between the direct and indirect gaps. Of course, its preparation may require the interposition of spacer layers. Furthermore, the issues connected with cross section or the oscillator strength for the direct transition may still render that superlattice unusable for optoelectronic devices. The direct transition energies from the highest valence-band state to the first, third, and fifth conduction-band states of $(Si)_4/(Ge)_4$ at Γ are 0.98, 1.55, and 2.37 eV, respectively. These calculated energies (with a constant shift of 0.5 eV) are in fair agreement with the observed direct optical transition[6] (0.76 ∓ 0.13, 1.25 ∓ 0.13, and 2.31 ∓ 0.12 eV).

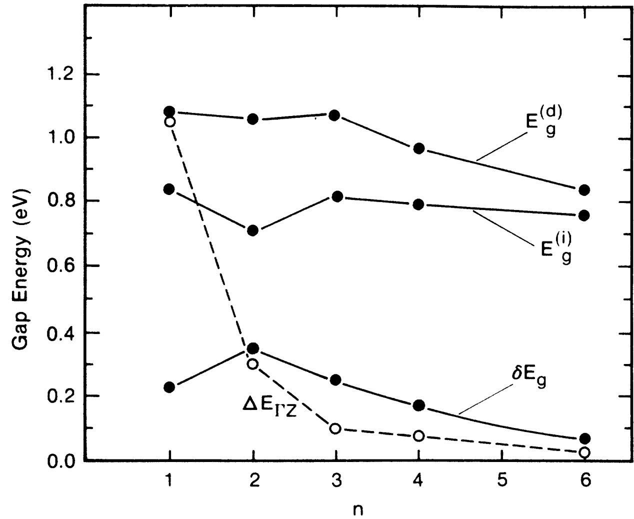

FIG. 10. Variation of the direct band gap ($E_g^{(d)}$), indirect ($E_g^{(i)}$) band gap, the difference between direct and indirect band gap (δE_g), and the width of the band along the ΓZ direction ($\Delta E_{\Gamma Z}$) as a function of the sublattice periodicity (n).

The variations of the direct and indirect gaps of $(Si)_n/(Ge)_n$ are summarized in Fig. 10. Since the lowest conduction-band state at Γ is a confined state, its energy has an inverse proportionality with n (the width of the sublattice), the exponent being between 1 and 2. This is the manifestation of the quantum size effect discussed above. It is seen that this trend breaks down for $n \leq 2$, where the multiple quantum-well structure is destroyed, and the lowest band has significant dispersion. An interesting feature we note in this figure is the energy difference between the direct and indirect gap, δE_g. All structures we studied are found to be indirect band-gap semiconductors. However, δE_g continues to decrease with increasing n, and is only 0.07 eV for $n=6$.

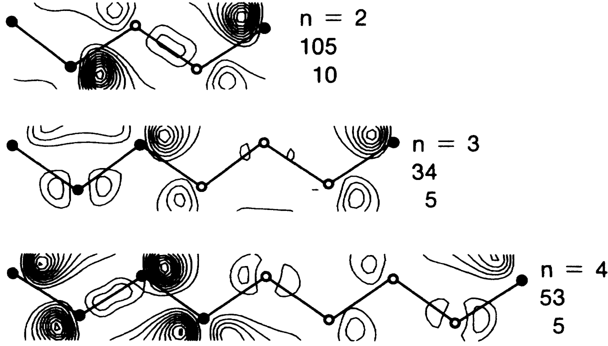

FIG. 11. Charge densities of the first conduction-band state of $(Si)_n/(Ge)_n$ ($n=2$, 3, and 4) along ΓZ. Upper and lower numerals at each panel are the values of maximum charge density and contour spacing in 10^{-4} a.u., respectively.

B. Charge-density analysis

We now focus on the important individual states at certain symmetry points of the SBZ, and examine their charge distribution. First we address the question of how the multiple quantum-well structure with confined states is developed. A pictorial demonstration of the confinement (or localization) of the lowest conduction-band states along ΓZ is presented by showing the charge distribution of states in Fig. 11. The lowest state for $(Si)_2/(Ge)_2$ is an interface state, which is localized between the adjacent Si and Ge layers. By going to $(Si)_3/(Ge)_3$ the charge distribution of this state shifts towards the Si sublattice, but still has significant weight at the interface. In the $(Si)_4/(Ge)_4$ structure, the confinement of electrons in the Si sublattice is, however, nearly complete. Concomitant with the confinement, the corresponding band becomes flat. The contour plots of the states at Γ are presented in Fig. 12 for $(Si)_4/(Ge)_4$. The top three states of the valence band have relatively high weight in the Ge sublattice. Clearly, these states cannot be considered as highly localized confined states. Since the calculated band offset for the valence band was reported[19] to be 0.84 eV (the average value being 0.54 eV), the character of these three states can be explained by the quantum size effect.[42–44] The smaller the width of the quantum well, the lower the energy of the highest hole state. It means that states confined in a small region have to increase their kinetic energies. Since the effective masses of the states at the maximum of the Ge valence band are $0.34m_0$, $0.043m_0$, and $0.08m_0$, they yield significant size effect even if the full width of the Ge sublattice is considered to be a quantum well. This effect becomes even more significant when the graded interface is taken into account. Therefore, in view of the calculated value for the valence-band offset, the confinement of the states near the maximum of the valence band is not expected for $n \lesssim 12$. Of course, in $(Si)_m/(Si_{1-x}G_x)_n$, for large n and m the hole states become easily confined.

The band offset at the conduction band[19] is ~ 0.28 eV, for the $\Delta_{c,1}$. At this minimum the transverse effective mass of the Si, m_t^* is small and is only $0.19m_0$. Given a small superlattice periodicity, the small effective mass imposes a large size effect. Consequently, the states around this minimum cannot be confined (in spite of the fact that they have the lowest energy in the conduction band). The contour plots of this state show clearly the extended nature of this particular state, and thus supports our arguments based on simple quantum-well picture. We also examined the states with $\mathbf{k}_{(\Delta_{c,1})}+\mathbf{k}_\perp$, and found significant dispersion and delocalized charge density. The lowest two states at Γ (but above $\Delta_{c,1}$) are strongly localized

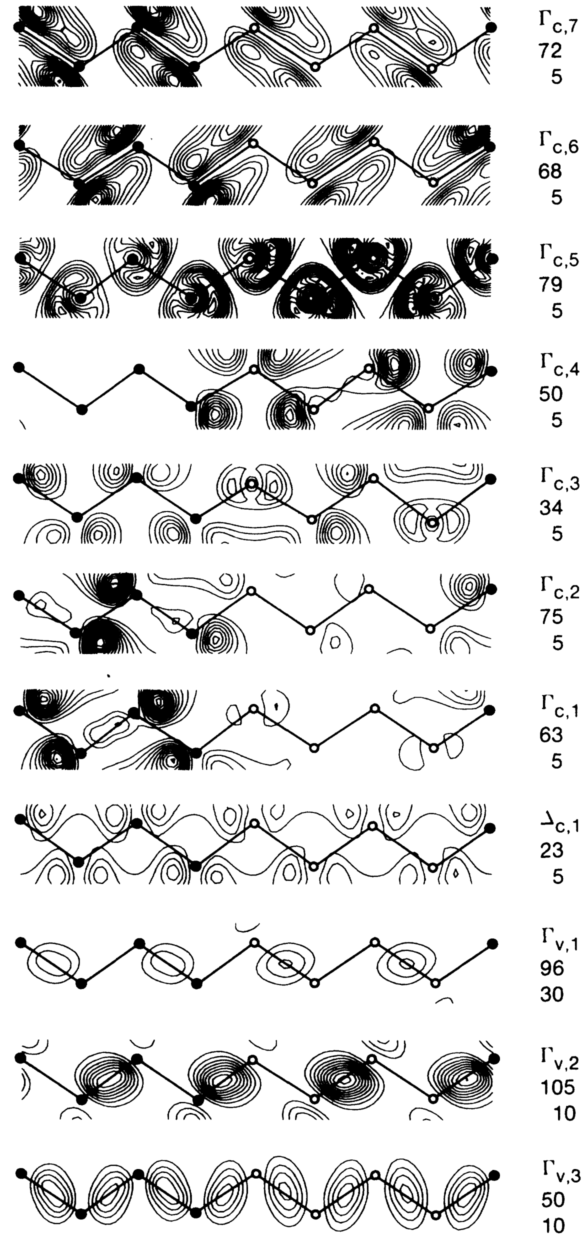

FIG. 12. Charge-density contour plots of the valence- and conduction-band states of $(Si)_4/(Ge)_4$ at Γ. Upper and lower numerals indicate the value of the maximum charge density and contour spacing, respectively.

(confined) in the Si sublattice. These are the states producing the flat bands along ΓZ shown in Fig. 8. Since upon the zone folding the longitudinal effective mass of Si (at $\Delta_{c,1}$), which is close to m_0, enters into the effective-mass Hamiltonian, the quantum size effect is much smaller than that for the extended, lowest conduction-band state discussed above. Depending on the alignment of particular bands, the localization of the higher-lying states alternates between two sublattices. Excepting $\Gamma_{c,5}$, which derives from the $\overline{\Gamma}_{2'}$, other states shown in Fig. 12 are evolved from the folding of bulk bands along $\overline{\Delta}$. The contour plots of the states at Γ for $(Si)_6/(Ge)_6$ are presented in Fig. 13. Owing to the increased sublattice width, and thus decreased quantum size effect, the localization of the hole states, and the degree of confinement of the conduction-band states are slightly increased. For $(Si)_6/(Ge)_6$ the bands along $\overline{\Delta}$ experience more folding than those in $(Si)_4/(Ge)_4$. Therefore, we see more folding states below the $\Gamma_{c,7}$ state of $(Si)_6/(Ge)_6$ as compared to the equivalent $\Gamma_{c,5}$ state of $(Si)_4/(Ge)_4$ in Fig. 12. Interestingly, the character and the charge distribution of these states are reminiscent of those shown in Fig. 12. This suggests that the alignment of the bands does not change significantly by increasing n from 4 to 6. However, at least the order of localization is strongly affected in the superlattice $(Si)_n/(Ge)_m$ with $n \neq m$.

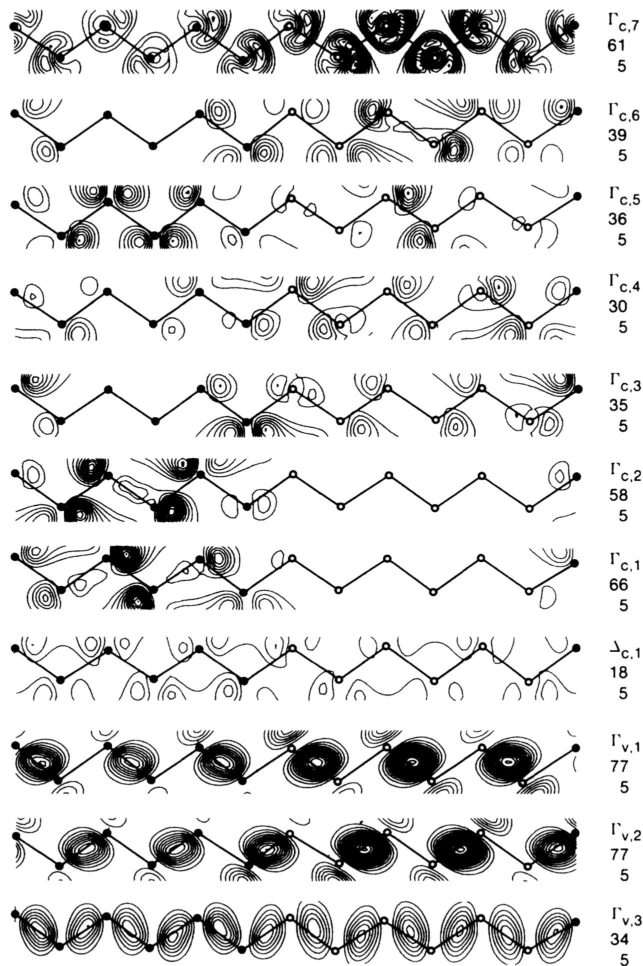

FIG. 13. Charge-density contour plots of the valence- and conduction-band states of $(Si)_6/(Ge)_6$ at Γ. Upper and lower numerals indicate the value of the maximum charge density and contour spacing, respectively.

The important conclusion we draw from Figs. 12 and 13 is that a single quantum-well structure within the effective-mass approximation cannot be applied for the superlattices with thin sublattice alternation. In this case each band should be considered individually. Or else the result has to be obtained from a complete SCF band calculation. It is seen that localized states can be found even far above the well (whose depth is obtained from the band offset). A pictorial demonstration of this emerges from the flat bands seen deep in the valence and conduction bands of $(Si)_4/(Ge)_4$ (see Fig. 8). Contour plots of these states are presented in Fig. 14. While the highest valence-band state along the ZR direction (but in a small region of the SBZ) is strongly localized in the Ge sublattice, the lowest conduction-band state is confined in Si. In contrast to that, the lowest conduction-band along the ΓR direction (again in a small region of the SBZ) is localized in the Ge sublattice. Certainly, in the superlattices with large sublattice alternations (where the bands experience frequent foldings, and thus the number of confined states are decreased), the lowest confined states can be obtained from the multiple quantum-well model.

VII. CONCLUSION

We have provided SCF total energy and force calculations to determine the minimum energy structure of pseudomorphic Si/Ge superlattices and alloys. Important results obtained from this study are summarized.

(i) The strained $(Si)_n/(Ge)_n$ superlattices are unstable relative to the decomposition into unstrained constituent crystals. In contrast to the lattice-matched heterostructures, the positive formation energy (per formula unit) linearly increases with the increasing superlattice periodicity. It is shown that for $n \geq 3$, the strain and interface contribution to the formation energy can be treated separately and linearly. The energy barrier to destroy the epitaxy by a defect (misfit dislocation) is estimated to be ~ 10 mRy cell.

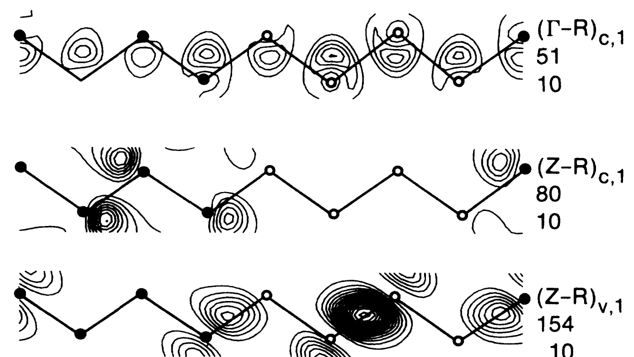

FIG. 14. Charge-density contour plots of the valence- and conduction-band states of $(Si)_4/(Ge)_4$ along ΓR and ZR.

(ii) The strained Si-Ge alloy, which also has positive enthalpy of formation, lowers energy by transforming into the strained rhombohedral structure. This is also only a metastable structure. The origin of this neostructural phase transition, in spite of the small amount of energy lowering, is sought in the short-range order involving rearrangements of Si and Ge atoms in the grown layer. The selective dimerization of the atoms in the topmost grown layer is proposed to induce the short-range order.

(iii) Confinement (or localization of states) indicates a type-II staggered band lineup. Lowest conduction-band states at Γ are localized at the interface of $(Si)_2/(Ge)_2$, but become confined in Si for $n > 3$. Because of the quantum size effect, the highest valence-band states are not fully localized in Ge. The same effect (due mainly to small electron effective mass) causes the lowest conduction-band states at Δ_{min} (which are located below the confined electron states) to have an extended nature. This is a new aspect of the band offset and quantum-well structure. Furthermore, localized states deep in the conduction and valence bands suggest that the electronic structure of the superlattices we investigated in the present study cannot be treated with a single quantum-well structure.

(iv) Among all structures ($1 \leq n \leq b$), $(Si)_2/(Ge)_2$ has displayed unusual properties which are not found in others. It has the lowest indirect band gap at M, and small formation energy.

(v) All $(Si)_n/(Ge)_n$ superlattices are found to be indirect band-gap semiconductors. The energy separation between the direct-indirect gap continues to decrease with increasing n, and is only 0.07 eV for $n = 6$. As a consequence, the superlattice has a quasidirect band-gap character. As can be seen from Fig. 10, δE_g approaches zero for $n > 6$. Since the strain in the Ge sublattice is a crucial factor[15,19] in the indirect-direct-gap transition, an optimum value for $a_{\parallel}$ has to be determined. In this situation both Si and Ge have to be strained. The variation of the sublattice thickness, for example $(Si)_m/(Ge)_n(Si)_1(Ge)_n$, or similar combinations in the alloy sublattice, may promote a direct gap. In an effort to improve the properties of Si an alternative way may be the growth of a dilute donor, and/or acceptor layers in the Si and Ge sublattices. The impurity bands obtainable from this doping may produce an extremum at Γ and modulate the band offset. The difficulty is, however, the diffusion of dopants into the sublattices.[45]

---

*Permanent address: Department of Physics, Bilkent University, Ankara, Turkey.

[1]E. Kasper, H. J. Herzog, and H. Kimble, Appl. Phys. **8**, 199 (1975).

[2]J. C. Bean, J. Vac. Sci. Technol. A **1**, 540 (1983); for a comprehensive review of the subject, see J. C. Bean, Phys. Today **39** (10), 36 (1986).

[3]A. T. Fiory, J. C. Bean, L. C. Feldman, and I. K. Robinson, J. Appl. Phys. **56**, 1227 (1984).

[4]R. People, J. C. Bean, D. V. Lang, A. M. Sergent, H. L. Störmer, K. W. Wecht, R. T. Lynch, and K. Baldwin, Appl. Phys. Lett. **45**, 1231 (1984).

[5]D. V. Lang, R. People, J. C. Bean, and A. M. Sergent, Appl. Phys. Lett. **47**, 1333 (1985).

[6]T. P. Pearsall, J. Bevk, L. C. Feldman, J. M. Bonar, J. P. Mannaerts, and A. Ourmazd, Phys. Rev. Lett. **58**, 729 (1987).

[7]S. Ciraci and I. P. Batra, Phys. Rev. Lett. **58**, 2114 (1987); in *Properties of Impurity States in Semiconductor Superlattices*, edited by C. Y. Fong, I. P. Batra, and S. Ciraci (Plenum, New York, 1988).

[8]S. Froyen, D. M. Wood, and A. Zunger, Phys. Rev. B **36**, 4547 (1987).

[9]R. People and S. A. Jackson, Phys. Rev. B **36**, 1310 (1987).

[10]S. Ellialtioglu, O. Gulsere, and S. Ciraci, in *Physics, Fabrication and Applications of Multilayered Structures*, edited by P. Dhez (Plenum, New York, 1987); S. Ciraci, O. Gulseren, and S. Ellialtioglu (unpublished); L. Brey and C. Tejedor, Phys. Rev. Lett. **59**, 1022 (1987).

[11]A. Ourmazd and J. C. Bean, Phys. Rev. Lett. **55**, 765 (1985).

[12]J. L. Martins and A. Zunger, Phys. Rev. Lett. **56**, 1400 (1986).

[13]T. F. Keuch, M. Mäenpä, and S. S. Lau, Appl. Phys. Lett. **39**, 245 (1981).

[14]G. Margaritando, A. D. Katnani, N. G. Stoffel, R. R. Daniels, and Te-Xiu Zhao, Solid State Commun. **43**, 163 (1982).

[15]G. Abstreiter, H. Brugger, T. Wolf, H. Jorke and H. Herzog, Phys. Rev. Lett. **54**, 2441 (1985).

[16]W. A. Harrison, J. Vac. Sci. Technol. **14**, 1016 (1987); J. Vac. Sci. Technol. B **3**, 1231 (1985).

[17]W. A. Harrison and J. Tersoff, J. Vac. Sci. Technol. B **4**, 1068 (1986).

[18]J. Tersoff, Phys. Rev. B **30**, 4874 (1984).

[19]C. H. van de Walle and R. M. Martin, J. Vac. Sci. Technol. B **3**, 1256 (1985); Phys. Rev. B **34**, 5621 (1986).

[20]Su-Huai Wei and A. Zunger, Phys. Rev. Lett. **59**, 144 (1987).

[21]I. Morrison, M. Jaros, and K. B. Wong, Phys. Rev. B **35**, 9693 (1987).

[22]S. Ciraci and I. P. Batra, Phys. Rev. B **36**, 1225 (1987).

[23]I. P. Batra, S. Ciraci, and J. Nelson, J. Vac. Sci. Technol. B **5**, 1300 (1987).

[24]M. Schlüter, J. R. Chelikowsky, S. G. Louie, and M. L. Cohen, Phys. Rev. B **12**, 4200 (1975).

[25]J. Ihm, A. Zunger, and M. L. Cohen, J. Phys. C **12**, 4409 (1979); M. T. Yin and M. L. Cohen, Phys. Rev. Lett. **45**, 1004 (1980).

[26]C. B. Bachelet, D. R. Hamann, and M. Schlüter, Phys. Rev. B **26**, 419 (1982).

[27]D. M. Ceperley and B. J. Alder, Phys. Rev. Lett. **45**, 566 (1980).

[28]J. P. Perdew and A. Zunger, Phys. Rev. B **23**, 5048 (1981).

[29]See, for the method and related references, I. P. Batra, S. Ciraci, G. P. Sirivastava, J. S. Nelson, and C. Y. Fong, Phys. Rev. B **34**, 8246 (1986).

[30]P. Bendt and A. Zunger, Phys. Rev. Lett. **50**, 1684 (1983).

[31]P. N. Keating, Phys. Rev. **145**, 637 (1966).

[32]F. J. Himpsel and D. E. Eastman, J. Vac. Sci. Technol. **16**, 1297 (1979); M. T. Yin and M. L. Cohen, Phys. Rev. B **24**, 2303 (1981).

[33]F. F. Abraham and I. P. Batra, Surf. Sci. **163**, L572 (1985),

and references therein.
[34]K. C. Pandey, *Proceedings of the XVII International Conference on the Physics of Semiconductors, San Francisco, 1984,* edited by D. J. Chadi and W. A. Harrison (Springer-Verlag, New York, 1985), p. 55.
[35]R. M. Tromp, R. J. Hamers, and J. E. Demuth, Phys. Rev. Lett. **55**, 1303 (1985).
[36]J. A. Kubby, J. E. Griffith, R. S. Becker, and J. S. Vickers, Phys. Rev. B **36**, 6079 (1987).
[37]I. P. Batra, Phys. Rev. B **29**, 7108 (1984); also see I. P. Batra and S. Ciraci, *ibid.* **29**, 6419 (1984).
[38]M. Cardona, G. Harbecke, O. Madelung, and U. Rössler, in *Physics of Group IV Elements and III-V Compounds,* Vol. 17a of *Landolt-Börnstein: Numerical Data and Functional Relationships in Science and Technology,* edited by O. Madelung (Springer-Verlag, New York, 1982), Group III.
[39]R. Hulthen and N. C. Nilsson, Solid State Commun. **18**, 1341 (1976).
[40]L. Esaki and R. Tsu, IBM J. Res. Dev. **14**, 61 (1970).
[41]M. Chandrasekhar and F. H. Pollak, Phys. Rev. B **15**, 2127 (1977).
[42]R. Dingle, in *Festkörperprobleme, Advances in Solid-State Physics,* edited by H. J. Queisser (Pergamon, Oxford, 1975), Vol. XV, p. 21.
[43]T. Ando, A. B. Fowler, and F. Stern, Rev. Mod. Phys. **54**, 437 (1982).
[44]S. Erkoc and S. Ciraci, Phys. Rev. B **34**, 4360 (1986).
[45]A. Zrenner and F. Koch, *Properties of Impurity States in Semiconductor Superlattices,* edited by C. Y. Fong, I. P. Batra, and S. Ciraci (Plenum, New York, 1988).

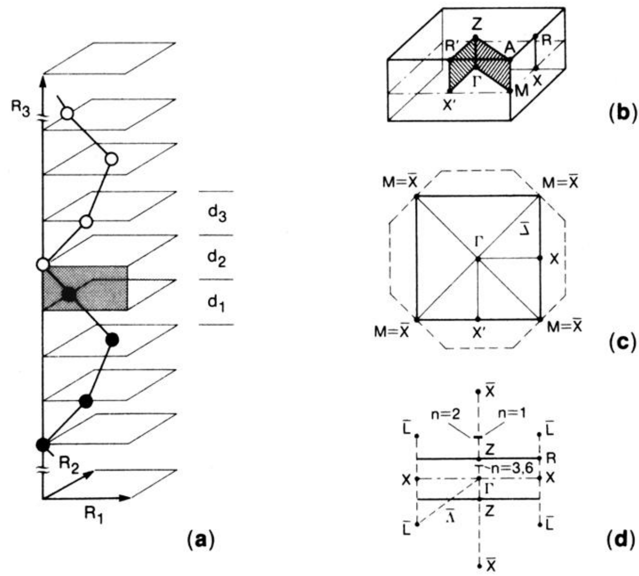

FIG. 1. (a) Tetragonal unit cell of the strained $(\mathrm{Si})_n/(\mathrm{Ge})_n$ superlattice with the solid and open circles denoting the position of Si and Ge atoms, respectively. $R_1=R_2=a^0_{\mathrm{Si}}/\sqrt{2}$ and $d_1=a^0_{\mathrm{Si}}/4$. R_3, d_2, and d_3 are obtained by minimization of the total energy. In all unit cells the first Si atom starting from the Si sublattice is located at the corner of the basal square of the tetragon. (b) Perspective view; (c) cross section through the horizontal central plane with dashed lines delineating the fcc BZ; (d) cross section through the vertical plane of the tetragonal superlattice Brillouin zone. The relation to the fcc BZ points labeled by the bar is indicated. ($\Gamma\bar{X}=2\pi/a^0_{\mathrm{Si}}$ and $X\bar{L}=\pi/a^0_{\mathrm{Si}}$.)